

PACS numbers: 42.55.Rz; 42.70.Hj; 81.05.Je; 42.25.Ja
DOI: 10.1070/QE2011v041n02ABEH014337

Polarisation dynamics of a Nd:YAG ceramic laser

P.A. Khandokhin, I.V. Ievlev, Yu.S. Lebedeva, I.B. Mukhin, O.V. Palashov, E.A. Khazanov

Abstract. **We report an experimental study of the polarisation dynamics of a dual-polarisation microchip Nd:YAG ceramic laser. Our results demonstrate dual-polarisation operation of the polycrystalline Nd:YAG laser. The low-frequency dynamics in this regime involves three types of relaxation oscillations, two of which are responsible for antiphase dynamics of the intensities of orthogonally polarised modes. Linearly polarised pump light induces gain anisotropy in the Nd:YAG ceramic, as in Nd:YAG single-crystal lasers. We present a comparative analysis of the behaviour of orthogonally polarised modes in Nd:YAG single-crystal lasers and the Nd:YAG ceramic laser, with a random orientation of the crystallographic axes in each grain (microcrystal), describe a technique for evaluating the total cavity loss from the relaxation oscillation spectrum and compare single-crystal and ceramic active elements. Experimental evidence is presented for gain anisotropy, loss anisotropy and phase anisotropy in ceramic and single-crystal microchip lasers.**

Keywords: *Nd:YAG ceramics, polarisation mode, relaxation oscillations, pump-induced gain anisotropy, Fabry–Perot cavity, microchip lasers, thermally induced depolarisation, thermal lensing.*

1. Introduction

Starting in about 1995, there was an explosive growth in the study of polycrystalline (ceramic) active Nd:YAG elements [1]. A rather large number of reports have since been devoted to the study of Nd:YAG ceramic active elements [1–14]. Ceramics have a number of important advantages, including a high production rate and the possibility of fabricating large ceramic bodies. Crystal growth by the Czochralski technique has a number of drawbacks in comparison with ceramic fabrication techniques, such as low growth rates, small crystal dimensions and relatively high cost. Currently, there are Nd:YAG ceramic bodies with an aperture as large as 1 m [3, 15, 16], which far exceeds the dimensions of the largest single crystals. Note that, in contrast to the quality of Nd:YAG crystals, that of large Nd:YAG ceramic bodies varies very little from their centre to their periphery, and the dopant concentration does not vary along the bodies. These advantages allow Nd:YAG ceramics to be employed in high-power laser systems. Considerable research effort has been focused on the optical properties (absorption, fluorescence spectra, depolarisation of light) and thermal behaviour of Nd:YAG ceramics with different doping levels and dynamic effects [1–12].

Kawai et al. [2] investigated in detail the dynamic behaviour and output beam characteristics of a laser-pumped microchip Nd:YAG ceramic laser and examined the effect of the fine structure of the ceramic, composed of single-crystal grains ~ 50 μm in average size, on the mode composition of the laser output. They observed unstable lasing with a large number of transverse modes identical in their spatial structure along the cavity axis. Laser beam polarisation was not examined in that study. On the other hand, dual polarisation would be expected in lasers with isotropic cavities (fibre lasers [17–19] and Nd:YAG single-crystal lasers [20–22]).

There is clear evidence [18–22] that linearly polarised pump light induces gain anisotropy: the intensities of orthogonally polarised modes depend on the pump beam polarisation. In each polarisation component, one or several longitudinal modes are generated. The set of longitudinal modes identical in field polarisation are commonly referred to as a supermode or simply a polarisation mode [17]. In addition to high-frequency in-phase relaxation oscillations, inherent in all types of lasers with an inertial active medium, low-frequency relaxation oscillations are identified [18–22] that are out of phase in each polarisation mode. To date, no such experiments have been performed with ceramic active elements. The purpose of this work was to study the fluctuation and polarisation properties of a microchip Nd:YAG ceramic laser pumped with linearly polarised light.

2. Experimental setup

Figure 1 shows a schematic of the experimental setup we used. Linearly polarised radiation from a laser diode (LD) was focused by lenses L1 and L2 onto an active element (Nd:YAG ceramic or single crystal) in the form of a plane-parallel plate about 8 mm in diameter and 2 mm in thickness. The plate had 1064-nm dielectric mirror coatings on both end faces and operated as a microchip laser. The coating on the input face was antireflective at 810 nm (pump wavelength) and highly reflective ($\sim 99.7\%$) at 1064 nm (laser wavelength). The coating on the output face was $\sim 95\%$ reflective at the pump wavelength and $\sim 99\%$ reflective at the laser wavelength. The active element was mounted in a holder (Fig. 1), which ensured translation along the x axis, normal to the laser beam propagation direction. A half-wave plate placed in the pump beam was used to control the pump beam polarisation direction (angle Ψ_P). A filter (F) at the Nd:YAG laser output served to eliminate the residual pump light in the data acquisition

P.A. Khandokhin, I.V. Ievlev, Yu.S. Lebedeva, I.B. Mukhin, O.V. Palashov, E.A. Khazanov Institute of Applied Physics, Russian Academy of Sciences, ul. Ul'yanova 46, 603950 Nizhnii Novgorod, Russia; e-mail: khando@appl.sci-nnov.ru

Received 2 April 2010; revision received 2 November 2010
Kvantovaya Elektronika **41** (2) 103–109 (2011)
Translated by O.M. Tsarev

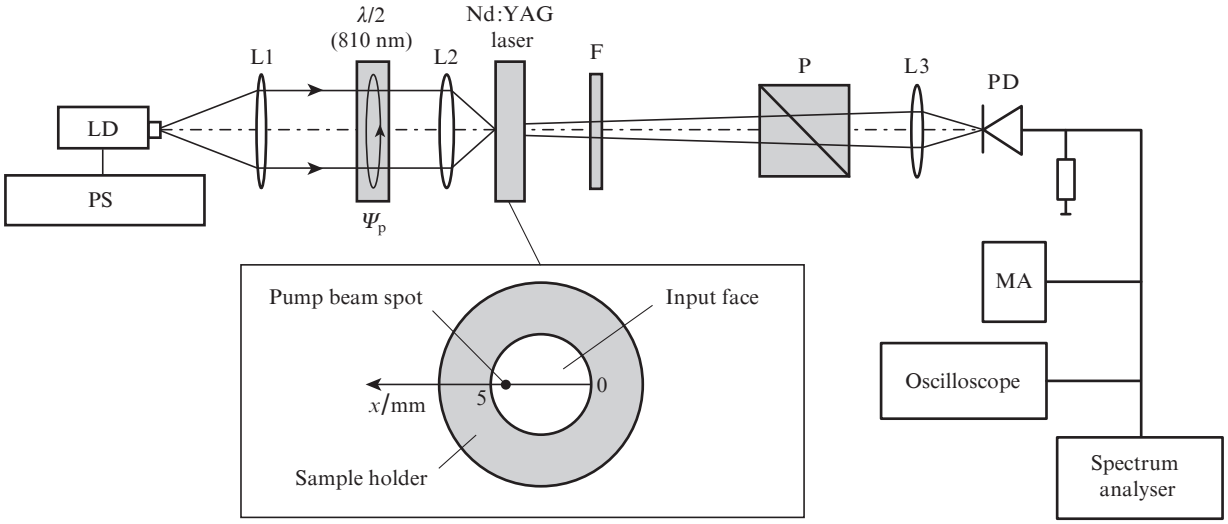

Figure 1. Schematic of the experimental setup: (PS) pump laser power supply; (LD) 810-nm pump laser diode; (L1 – L3) focusing lenses; (F) 810-nm attenuation filter; (P) polarising cube (Glan prism); (PD) photodiode; (MA) microammeter.

channel. The laser beam was incident on a Glan polariser (P), which was used to observe individual polarisation modes. Carefully focusing the radially symmetric pump beam onto the input face of the crystal, we achieved lasing in the fundamental transverse mode TEM_{00} with a beam divergence of $\sim 8.6\times10^{-3}$ rad, i.e. the beam diameter was 40 μm.

The Nd^{3+} content of the Nd:YAG ceramic was 2.3 at%, which is about twice the typical doping level in Nd:YAG crystals. The laser output was analysed using a low-frequency spectrum analyser, oscilloscope and power meter. We observed two orthogonal linearly polarised TEM_{00} modes, which were identical in transverse spatial structure.

The intensity ratio of the orthogonally polarised modes was varied by either scanning the active element with the pump beam or changing its polarisation direction. Measurement results were compared to those for an [001]-oriented microchip Nd:YAG single-crystal laser with a crystal (cavity) length of 2 mm. The Nd^{3+} content of the crystal was ~1 at%.

3. Experimental results

3.1. Relaxation oscillation spectrum

The Nd:YAG ceramic laser output was found to comprise two polarisation modes. The mode composition of the laser beam (more precisely, single- or dual-polarisation operation) was inferred from the intensity fluctuation spectrum for the two orthogonal polarisations: the presence of only one high-frequency relaxation peak in the intensity fluctuation spectrum was considered evidence of single-mode operation. In our experiments, we examined the effect of pump beam polarisation on the intensity of the polarisation modes of the Nd:YAG laser. The technique used to determine the polarisation mode orientation was described in earlier reports on the dynamics of dual-polarisation lasers [18–22]. As a rule, a strong polarisation mode corresponded to the analyser orientation that maximised the transmitted beam intensity. A weak polarisation mode corresponded to the orthogonal analyser orientation, which minimised the transmitted beam intensity.

The present results for the Nd:YAG ceramic laser demonstrate that the intensity fluctuation spectra of both polarisation modes show three types of relaxation oscillations in the form of resonances at frequencies f_1 to f_3 (Fig. 2). The high-frequency peaks at f_1 are due to in-phase intensity oscillations, and the low-frequency peaks at f_2 and f_3 arise from anti-phase intensity oscillations of the polarisation modes [22]. Owing to this, the total intensity fluctuation spectrum shows weak or no low-frequency relaxation oscillations. The presence of resonance peaks with maximum heights at frequencies f_2 and f_3 in the intensity fluctuation spectrum was considered an extra criterion for whether the analyser was accurately adjusted to the polarisation mode: a deviation of the analyser from this orientation reduced the height of the peaks. This behaviour of the polarisation relaxation oscillations in the intensity fluctuation spectrum of the Nd:YAG ceramic laser is identical to that in the spectrum of Nd:YAG single-crystal lasers (Fig. 2b) [20–22]. It is worth pointing out that the Nd:YAG ceramic laser output had high noise and was less stable than the Nd:YAG single-crystal laser output. In our experiments, its instability showed up as a deviation from the fundamental relaxation oscillation frequency f_1, which led to a relative change in frequency $\Delta f_1/f_1 \approx 0.1$. For the single crystal, the change was ~0.04. Figures 3a and 4a show the polarisation mode intensities and relaxation oscillation frequencies as functions of the pump parameter (ratio of the pump power P_p to the threshold pump power P_{th}):

$$A = P_p/P_{th}. \tag{1}$$

The pump threshold of the Nd:YAG ceramic laser was determined to be 411 mW. The pump beam polarisation was optimal for one of the polarisation modes (e.g. for that of intensity I_1). Near the lasing threshold ($1 < A < A_2$), we observed dual-polarisation laser operation. At pump parameters above the second lasing threshold ($A > A_2$), the orthogonal polarisation mode came into play, and resonance peaks emerged in the intensity fluctuation spectrum at the polarisation relaxation oscillation frequencies f_2 and f_3. Figures 3b and 4b present analogous data for a Nd:YAG single-crystal laser. The pump threshold of this laser, 230 mW, was lower than that of the ceramic laser. This may be due both to the reduction in quantum yield (luminescence quenching) with increasing neodymium

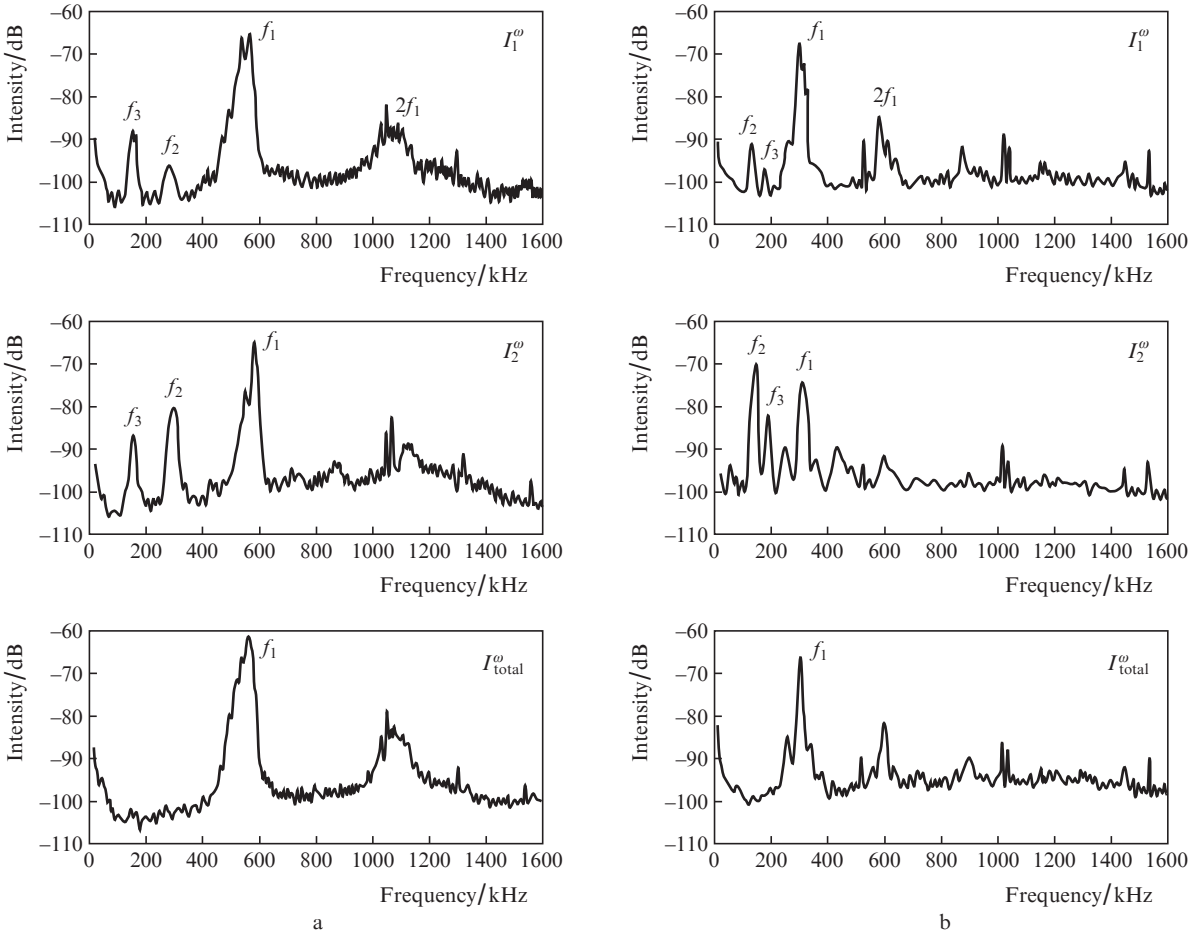

Figure 2. Intensity fluctuation spectra of the individual orthogonally polarised modes ($I^{\omega}_{1,2}$) and total intensity fluctuation spectra (I^{ω}_{total}) for Nd:YAG (a) ceramic and (b) single-crystal lasers.

concentration [23–25] and to the fact that ceramics have higher optical losses in comparison with crystals. The loss related to the active elements can be estimated from the in-phase relaxation oscillation frequency $f_1(A)$ using the well-known relation [26]

$$2\pi T_1 f_1 = \sqrt{G(A-1)}. \qquad (2)$$

Here T_1 is the population inversion relaxation time and $G = T_1/T_c$, where T_c is the field relaxation time in the cavity, dominated by the cavity loss. For Nd:YAG single crystals

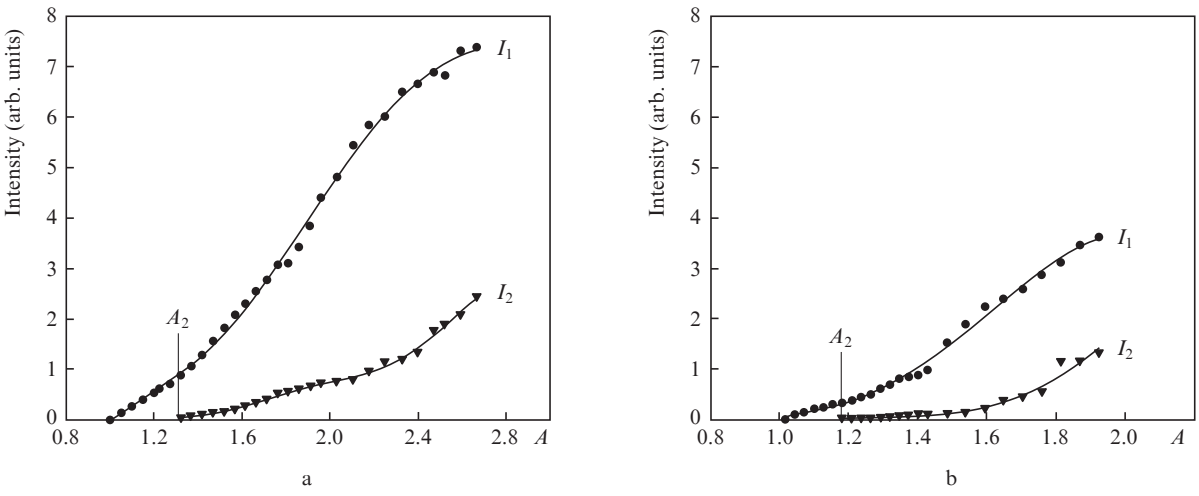

Figure 3. Polarisation mode intensities I_1 and I_2 as functions of the pump parameter, $A = P_p/P_{th}$, for Nd:YAG (a) ceramic and (b) single-crystal lasers.

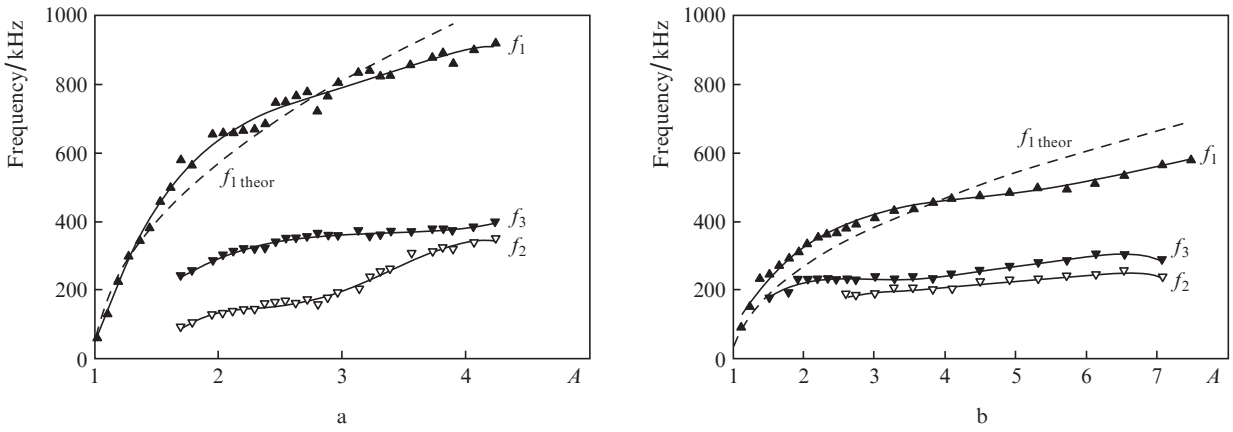

Figure 4. Relaxation oscillation frequencies as functions of the pump parameter A for Nd:YAG (a) ceramic and (b) single-crystal lasers. The dashed lines ($f_{1\,\mathrm{theor}}$) represent theoretical fits to (2) for the fundamental relaxation oscillation frequency vs. A data.

containing 1 at % Nd, $T_1 = 2.3\times10^{-4}$ s. With increasing active-ion concentration, the population inversion relaxation time decreases [23]. The T_1 of the ceramic studied here, containing 2.3 at % Nd, is $\sim 1.5\times10^{-4}$ s. From relation (2), we can find the photon lifetime in the cavity, T_c, which determines the cavity mode width:

$$\delta f \equiv (2\pi T_c)^{-1} = 2\pi f_1^2 T_1/(A-1). \tag{3}$$

At $A = 2$ and $f_1 \approx 600$ kHz, we have for the ceramic studied $\delta f \approx 340$ MHz. For the single crystal at $A = 2$ and $f_1 \approx 250$ kHz, we obtain $\delta f \approx 90$ MHz. Knowing the mode width, one can evaluate the cavity loss coefficient [27]:

$$\alpha = 2\pi n \delta f/c + (1/L)\ln\sqrt{R_1 R_2}, \tag{4}$$

where c is the speed of light; n is the refractive index of the medium in the cavity; L is the cavity length; and R_1 and R_2 are the reflectivities of the input and output mirrors of the cavity, respectively. Under the experimental conditions of this study, the total loss, $2\pi n\delta f/c$, is $\sim(0.13\pm0.03)$ cm^{-1} in the ceramic laser and just (0.034 ± 0.006) cm^{-1} in the single-crystal laser. The transmission loss of the mirrors, $-(1/L)\ln(R_1R_2)$, is 0.033 cm^{-1} for the single crystal and 0.043 cm^{-1} for the ceramic. Therefore, the loss in the single crystal is essentially zero, whereas that in the ceramic is $\alpha_{\mathrm{ceram}} \approx (0.09\pm0.03)$ cm^{-1}. Thus, the loss in the ceramic active element is about twice the useful loss, and the loss in the single crystal is well below the useful loss.

The origin of the high losses in the ceramic active element is not yet clear. They may be related to the quality of the material, its polycrystalline structure and thermal effects (thermally induced depolarisation and thermal lensing). Let us estimate the associated losses. Proceeding as in earlier studies [28, 29], we obtain an expression for the round-trip loss of cavities in the form of [001]- and [111]-oriented crystals:

$$\gamma_{\mathrm{total}} = 2\alpha_T L = \gamma_{\mathrm{ani}} + \gamma_{\mathrm{i}}, \tag{5}$$

where

$$\gamma_{\mathrm{ani}}([001]) = 0.017(1+\xi^2)p^2;$$

$$\gamma_{\mathrm{ani}}([111]) = 0.034\left(\frac{1+2\xi}{3}\right)^2 p^2;$$

$$\gamma_{\mathrm{i}} = \begin{cases} 0.067 p_{\mathrm{i}}^2 \text{ (with no thermal lensing compensation)}, \\ 0.0044 p_{\mathrm{i}}^2 \text{ (with compensation)}; \end{cases}$$

$$p = \frac{QP_{\mathrm{h}}}{\lambda\kappa}; \quad p_{\mathrm{i}} = 2\frac{PP_{\mathrm{h}}}{\lambda\kappa}; \quad \xi = \frac{2p_{44}}{p_{11}-p_{12}};$$

$$Q = \alpha_{\mathrm{L}}\frac{n^3}{4}\frac{1+\nu}{1-\nu}(p_{11}-p_{12});$$

$$P([001]) = \frac{\mathrm{d}n}{\mathrm{d}T} - \alpha_{\mathrm{L}}\frac{n^3}{4}\frac{1+\nu}{1-\nu}(p_{11}+p_{12});$$

$$P([111]) = P([001]) - \frac{\xi-1}{3}Q;$$

α_T is the thermal loss coefficient; P_{h} is the heat release rate; $\alpha_{\mathrm{L}} = 8\times10^{-6}$ is the linear thermal expansion coefficient; $\nu = 0.3$ is Poisson's ratio; p_{ij} are the photoelasticity tensor components (photoelastic coefficients) in the two-index notation ($p_{11} = -0.029$, $p_{12} = 0.0091$, $p_{44} = -0.0615$); Q and P are the thermo-optic constants of the medium [30], characterising the thermally induced anisotropy and the isotropic distortion, respectively; $\mathrm{d}n/\mathrm{d}T = 9\times10^{-6}$ K^{-1}; and $\kappa \approx 10$ W m^{-1} K^{-1}. The expressions for [111]-oriented crystals can be adjusted to ceramics by formally replacing ξ by ξ_{eff} in the relations for the anisotropic loss γ_{ani} [13, 31] and isotropic loss γ_{i} [32]. The γ_{total} of [001]- and [111]-oriented YAG crystals ($\xi = 3.2$) is close to that of the ceramic.

In deriving the formulas above, we assumed for simplicity that the pump intensity profile coincided with the cavity mode profile. Thermal lensing compensation then means that the cavity mode fully adjusts to the parabolic component of the thermal lens and, hence, parabolic aberration makes no contribution to the loss. This compensation is only partial. Since its exact magnitude under typical experimental conditions is rather difficult to accurately evaluate, we will specify a loss range: from the absence of compensation to complete compensation. From the above experimental data, we obtain $\alpha_{T\mathrm{ceram}} = 3\times10^{-3}$ to 3×10^{-2} cm^{-1} and $\alpha_{T\mathrm{crys}} = 10^{-3}$ to 10^{-2} cm^{-1}.

The lower loss in the single crystal is due to the lower lasing threshold and, hence, slower heat release rate. Note that the above estimates do not take into account the losses caused by the bending of the end faces of the active element or by electronic thermal lensing [33]. Analysis in earlier studies [13, 31, 32] indicates that the loss due to specific ceramic effects at a relatively small heat release ($p \approx 0.1$) is negligible. In that analysis, however, the beam diameter was taken to considerably exceed the grain size of the ceramic. In the present experiments, they were comparable.

Thus, our estimates demonstrate that thermal effects make a significant contribution to the cavity loss. In addition, there are losses due to scattering (both in the bulk and on the surface of the active element), nonparallelism of the end faces and nonuniformity of the 'cold' photoelastic effect (see below).

It is of interest to compare the present results to earlier data. In particular, for the experimental conditions in Kawai et al. [2] (5 at% Nd ($T_1 = 0.6\times10^{-4}$ s), $A = 6.36$, $f_1 = 3.5$ MHz) we have $\delta f = 766$ MHz. The total loss, $2\pi n\delta f/c$, was ~ 0.16 cm^{-1}, and the transmission loss of the mirrors, $-(1/L)\ln(R_1R_2)$ ($L = 0.9$ mm, $R_1 = 0.999$, $R_2 = 0.99$), was ~ 0.06 cm^{-1}. Finally, we obtain $\alpha \approx 0.1$ cm^{-1}. Thus, the loss in the ceramic active element also exceeds the useful loss. Estimates analogous to those above give a thermal loss coefficient $\alpha_T = 4\times10^{-3}$ to 4×10^{-2} cm^{-1}, which also suggests that thermal effects make a significant contribution.

According to our experimental data, the relaxation oscillation frequencies f_1 to f_3 of both the single-crystal and ceramic lasers depend very little on Ψ_P.

3.2. Cavity anisotropy

When the pump beam was scanned over the surface of the Nd:YAG ceramic active element, we observed inhomogeneities in the form of individual grains. The dynamic behaviour of the laser varied from point to point: from steady-state lasing, with the above intensity fluctuation spectrum of the polarisation modes, to an unsteady state, including random lasing.

Figure 5 plots the lasing thresholds of the polarisation modes against the position of the pump beam spot on the input face (see the inset in Fig. 1) for the pump polarisation parallel to the polarisation of the strong mode (having the maximum intensity). As seen, the lasing thresholds of the modes depend significantly on the position of the pump beam spot on the active element, especially in the case of the ceramic.

We find that rotation of the plane of polarisation of the pump beam has no effect on the polarisation of the cavity eigenmodes but leads to antiphase variations in the intensities I_1 and I_2 of the polarisation modes with a 180° period (Fig. 6). The intensity difference between the polarisation modes in the ceramic far exceeds that in the single crystal.

The above results demonstrate that there are several types of cavity anisotropy: phase anisotropy, pump-induced gain anisotropy, loss anisotropy and pump absorption anisotropy. Note that the loss and gain in the ceramic are more anisotropic than those in the single crystal. Let us analyse the relevant data in greater detail.

First, the cavity eigenpolarisation direction is independent of pump polarisation. Because the thermal loss γ_{total} in (5) is independent of the beam polarisation direction, thermal effects cannot be responsible for the cavity loss anisotropy. Therefore, the cavity has phase anisotropy, which may only be due to the photoelastic effect caused by 'cold' (rather than thermal) stress in the active element. The phase anisotropy so much exceeds the pump-induced gain anisotropy (see below) that, even at an arbitrary pump polarisation direction, the cavity eigenpolarisations are governed by the phase anisotropy orientation.

Second, the thresholds for the two eigenpolarisations are determined mainly by the pump-induced gain anisotropy [22] because the lasing threshold for the mode whose polarisation is parallel to the pump polarisation is always lower than that for the mode whose polarisation is orthogonal to the pump polarisation (Fig. 5). This experimental finding cannot be accounted for by pump absorption anisotropy, cavity loss anisotropy or phase anisotropy.

Third, the fact that both the lasing thresholds and their difference are strong functions of the position of the pump beam spot on the cross section of the ceramic active element (Fig. 5a) suggests that there is gain or absorption anisotropy, which is very small in the single crystal. The absorption anisotropy can be interpreted in terms of a transverse spatial inhomogeneity of 'cold' mechanical stress, which leads to aberrations (and, hence, to losses), whose magnitude is governed by the refractive index change and depends on the orientation of the crystallographic axes in each grain. The gain anisotropy may also depend significantly on the orientation of the crystallographic axes. In both cases, a transverse displacement of the laser beam by the grain size (50–70 μm) changes the set of grains the laser beam passes through and the lasing thresholds (Fig. 5a).

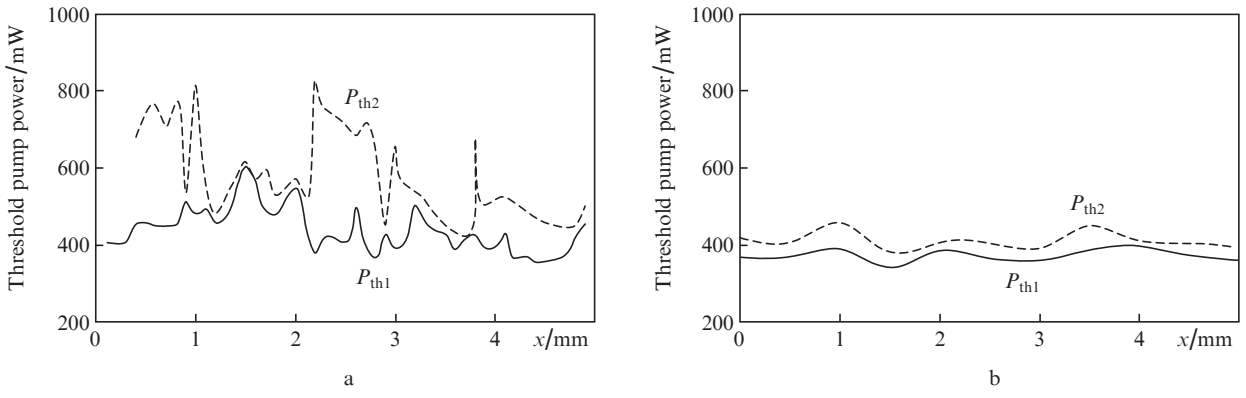

Figure 5. Lasing thresholds of the polarisation modes (P_{th1} and P_{th2}) vs. x (position of the pump beam spot on the input face, see Fig. 1) for Nd:YAG (a) ceramic and (b) single-crystal lasers.

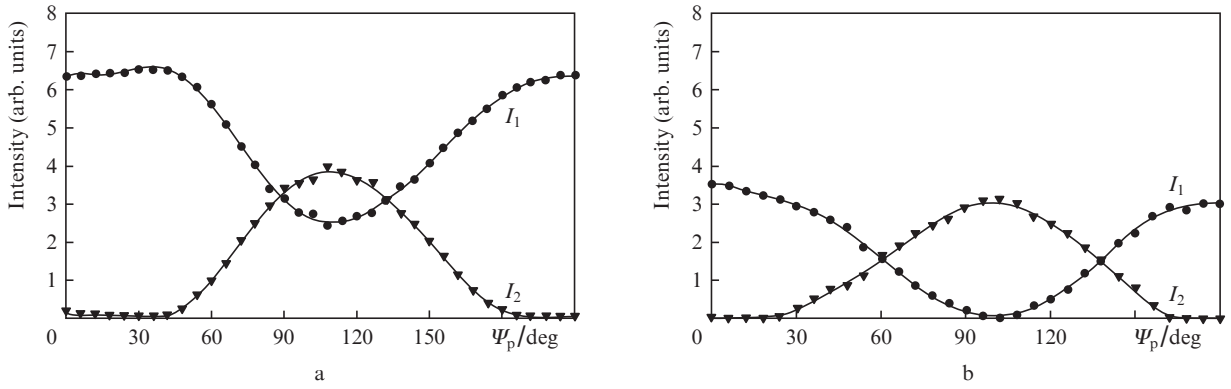

Figure 6. Intensities of the polarisation modes against the angle of the linear polarisation of the pump beam, Ψ_P, for Nd:YAG (a) ceramic and (b) single-crystal lasers.

Finally, Fig. 6 clearly demonstrates that the eigenpolarisations differ in intensity, especially in the ceramic. The underlying mechanisms are similar to those above.

An adequate model capable of evaluating cavity eigenpolarisations with all of the above types of anisotropy is difficult to construct for both the single-crystal and ceramic lasers. Future work will address this issue.

4. Conclusions

In our experiments, dual-polarisation operation has been demonstrated for both a microchip Nd:YAG ceramic laser and a Nd:YAG single-crystal laser.

The intensity fluctuation spectra of the two polarisation modes show three relaxation peaks, at frequencies f_1 to f_3. The relaxation peaks at frequencies f_2 and f_3 arise from small antiphase intensity oscillations of the orthogonally polarised modes. In the total intensity fluctuation spectrum of the dual-polarisation laser, the oscillations at these frequencies are compensated, and there is only the resonance peak at the in-phase relaxation oscillation frequency f_1.

Under the experimental conditions of this study, the orientations of the polarisation modes were independent of pump polarisation and were governed by the residual ('cold') birefringence, like in the Nd:YAG single-crystal laser. Only in the case of a fully isotropic cavity will the orientations of the polarisation eigenmodes of the laser follow the variation in pump beam polarisation, as was demonstrated by Kravtsov et al. [34]. In addition, the orientations of the polarisation modes were independent of the position of the pump beam spot on the input face of the active element.

Our experiments with a microchip laser based on a Fabry–Perot cavity revealed several types of anisotropy: phase anisotropy, pump-induced gain anisotropy, loss anisotropy and pump absorption anisotropy. The loss and gain anisotropy in the ceramic exceeds that in the single crystal and depends significantly on the orientation of the crystallographic axes in particular grains.

References

1. Ikesue A., Furusato I., Kamata K. *J. Am. Ceram. Soc.*, **78**, 225 (1995).
2. Kawai R., Miyasaka Y., Otsuka K., Ohtomo T., Narita T., Ko J.-Y., Shoji I., Taira T. *Opt. Express*, **12**, 2293 (2004).
3. Qi Y., Zhu X., Lou Q., Ji J., Jingxing Dong, Wei Y. *Opt. Express*, **13**, 8725 (2005).
4. Kracht D., Frede M., Wilhelm R., Fallnich C. *Opt. Express*, **13**, 6212 (2005).
5. Wei D., Takahashi S., Takamasu K., Matsumoto H. *Opt. Express*, **17**, 7011 (2005).
6. Lin G., Wei H., Hong-bo Z., Zhi-pei S., Cui D., Zu-yan X., Yong-Gang W., Xiao-Yu M. *Opt. Express*, **13**, 4085 (2005).
7. Mukhin I.B., Palashov O.V., Khazanov E.A., Ikesue A., Aung Y.L. *Opt. Express*, **13**, 5983 (2005).
8. Sträßer A., Ostermeyer M. *Opt. Express*, **14**, 6687 (2006).
9. Kracht D., Freiburg D., Wilhelm R., Frede M., Fallnich C. *Opt. Express*, **14**, 2690 (2006).
10. Omatsu T., Nawata K., Sauder D., Minassian A., Damzen M.J. *Opt. Express*, **14**, 8198 (2006).
11. Ikesue A., Aung Y.L. *J. Am. Ceram. Soc.*, **89**, 1936 (2006).
12. Lee S.-H., Kochawattana S., Messing G.L., Dumm J.Q., Quarles G., Castillo V. *J. Am. Ceram. Soc.*, **89**, 1945 (2006).
13. Khazanov E.A. *Opt. Lett.*, **27**, 716 (2002).
14. Ikesue A., Aung Y.L. *Nat. Phys.*, **2**, 721 (2008).
15. Lu J., Prabhu M., Xu J., Ueda K., Yagi H., Yanagitani T., Kaminskii A.A. *Appl. Phys. Lett.*, **77**, 3707 (2000).
16. Lu J., Song J., Prabhu M., Xu J., Ueda K., Yagi H., Yanagitani T., Kudryashov A. *Appl. Phys.*, **39**, 1048 (2000).
17. Bielawski S., Derozier D., Glorieux P. *Phys. Rev. A*, **46**, 2811 (1992).
18. Khandokhin P.A., Khanin Ya.I., Mamaev Yu.A., Milovskii N.D., Shirokov E.Yu., Bielawski S., Derozier D., Glorieux P. *Kvantovaya Elektron.*, **25**, 517 (1998) [*Quantum Electron.*, **28**, 502 (1998)].
19. Khandokhin P., Khanin Y., Mamaev Y., Milovsky N., Shirokov E., Bielawski S., Derozier D., Glorieux P. *Quantum Semiclassical Opt.*, **10**, 97 (1998).
20. Khandokhin P.A., Milovsky N.D., Mamaev Y.A., Ovchinnikov E., Shirokov E.Y. *Proc. SPIE–Int. Soc. Opt. Eng.*, **3682**, 53 (1998).
21. Bouwmans G., Segard B., Glorieux P., Khandokhin P.A., Milovsky N.D., Shirokov E.Y. *Radiophys. Quantum Electron.*, **47**, 813 (2004).
22. Ievlev I.V., Khandokhin P.A., Shirokov E.Yu. *Kvantovaya Elektron.*, **36**, 228 (2006) [*Quantum Electron.*, **36**, 228 (2006)].
23. Zverev G.M., Golyaev Yu.D. *Lazery na kristallakh i ikh primenenie* (Single-Crystal Lasers and Their Applications) (Moscow: Radio i Svyaz', 1994) p. 312.
24. Lupei V., Lupei A., Georgescu S., Diaconescu B., Taira T., Sato Y., Kurimura S., Ikesue A. *J. Opt. Soc. Am. B*, **19**, 360 (2006).
25. Merkle L.D., Dubinskii M., Schepler K.L., Hegde S.M. *Opt. Express*, **14**, 3893 (2006).
26. Khanin Ya. I. *Fundamentals of Laser Dynamics* (Cambridge: Cambridge International Science Publishing, 2006; Moscow: Nauka, 1999).
27. Yariv A. *Introduction to Optical Electronics* (New York: Holt, Rinehart & Winston, 1976; Moscow: Vysshaya Shkola, 1983).
28. Khazanov E.A., Andreev N.F., Mal'shakov A.N., Palashov O.V., Poteomkin A.K., Sergeev A.M., Shaykin A.A., Zelenogorsky V.V.,

Ivanov I., Amin R.S., Mueller G., Tanner D.B., Reitze D.H. *IEEE J. Quantum Electron.*, **40**, 1500 (2004).
29. Khazanov E.A. *Kvantovaya Elektron.*, **30**, 147 (2000) [*Quantum Electron*., **30**, 147 (2000)].
30. Mezenov A.V., Soms L.N., Stepanov A.I. *Termooptika tverdotel'nykh lazerov* (Thermal Optics of Solid-State Lasers) (Leningrad: Mashinostroenie, 1986) p. 199.
31. Kagan M.A., Khazanov E.A. *Kvantovaya Elektron.*, **33**, 876 (2003) [*Quantum Electron.*, **33**, 876 (2003)].
32. Snetkov I.L., Mukhin I.B., Palashov O.V., Khazanov E.A. *Kvantovaya Elektron*., **37**, 633 (2007) [*Quantum Electron.*, **37**, 633 (2007)].
33. Antipov O.L., Bredikhin D.V., Eremeykin O.N., Ivakin E.V., Savikin A.P., Sukhodolov A.V., Fedorova K.A. *Kvantovaya Elektron*., **36**, 418 (2006) [*Quantum Electron.*, **36**, 418 (2006)].
34. Kravtsov N.V., Lariontsev E.G., Naumkin N.I. *Kvantovaya Elektron.*, **34**, 839 (2004) [*Quantum Electron.*, **34**, 839 (2004)].